J-10.2 Higher Alluvial CEC of 7 meq/100 g

In order to evaluate the non-linearity of predicted response to CEC, the higher end of alluvium CEC was considered. This simulation was conducted to complete the alluvium CEC range from 2, 3, and 7 meq/100 g, and is based on the RI/BRA model presented in Section J-8.

J-10.2.1 Geochemical Evolution in the Alluvium

For comparison to the RI/BRA model, figures for the transport of total aqueous Sr, the amount of Sr-90 on exchange sites, and the resultant effective K_d are given in Figures J-10-13 through J-10-15. The aqueous phase concentrations are lower than predicted in the RI/BRA model in response to the higher CEC. Simultaneously, the total Sr-90 associated with exchange sites is slightly higher, with most of the Sr-90 existing on exchange sites at higher elevations in the alluvium. The resultant effective partition coefficient is significantly higher, with the highest values coinciding with the center of aqueous phase activity.

After 5, 10, 15, and 20 years, the total Sr-90 that has entered the vadose zone under the alluvium is 1773, 6378, 6393, and 6403 Curies, respectively as shown in Figure J-10-16. It is readily apparent that over the entire range of CEC expected to exist in the INTEC alluvium, the initial rapid release of Sr-90 occurs within the first 5 years. With the higher CEC, a larger fraction (9497 Ci vs. 3564 Ci) remains in the alluvium after 20 years as shown in the summary Figure J-10-16. Over the entire range examined here, the amount of transported Sr-90 (Figure J-10-13) is a nearly linear function of CEC.

The majority of Sr-90 remaining in the alluvium exists at shallow depths on the exchange sites as shown in Figures J-10-14 and J-10-16. The largest change in the distribution of Sr-90 on the exchange sites occurs soon after the CPP-31 release. During the first five years, the slightly mobile Sr-90 migrates from the initial release location and partitions onto the solids. As this redistribution occurs, there is an initial rise in effective K_d, reaching a peak value of 20 mL/g at 12 years, followed by a slow decrease in Sr-90 on the exchange sites as the other cations in solution leave the alluvium. Increasing the CEC has increased the effective K_d for the Sr-90 remaining in the alluvium to 17 mL/g compared to 2 mL/g in the base case as shown in Figures J-10-13 and J-10-16. The decrease in initial released activity and large increase in effective K_d is reflected in the resulting peak vadose zone and aquifer concentrations.

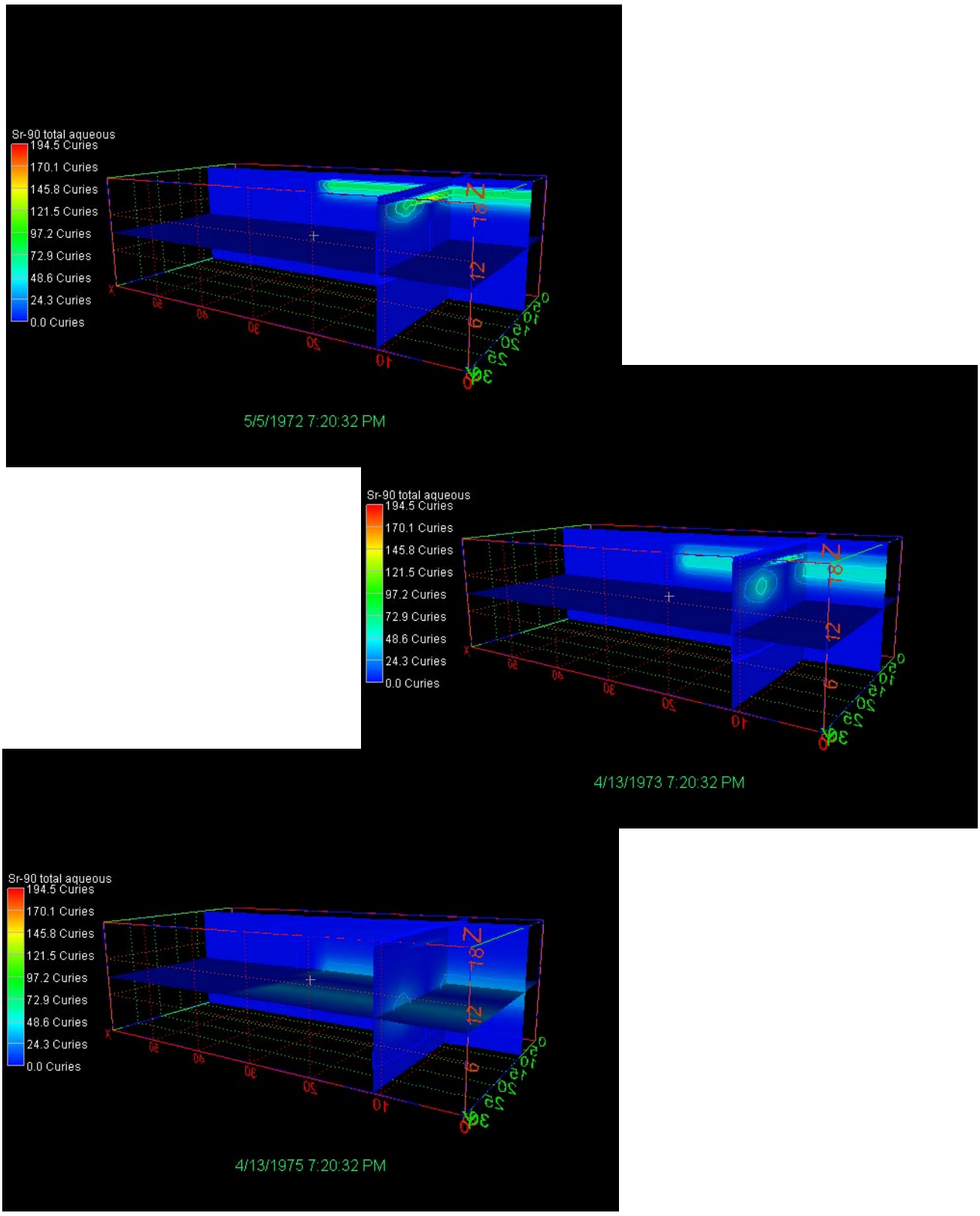

Figure J-10-13. Total aqueous-phase Sr-90 0.5, 1.5, and 3 years after CPP-31 release with CEC = 7 meq/100 g.

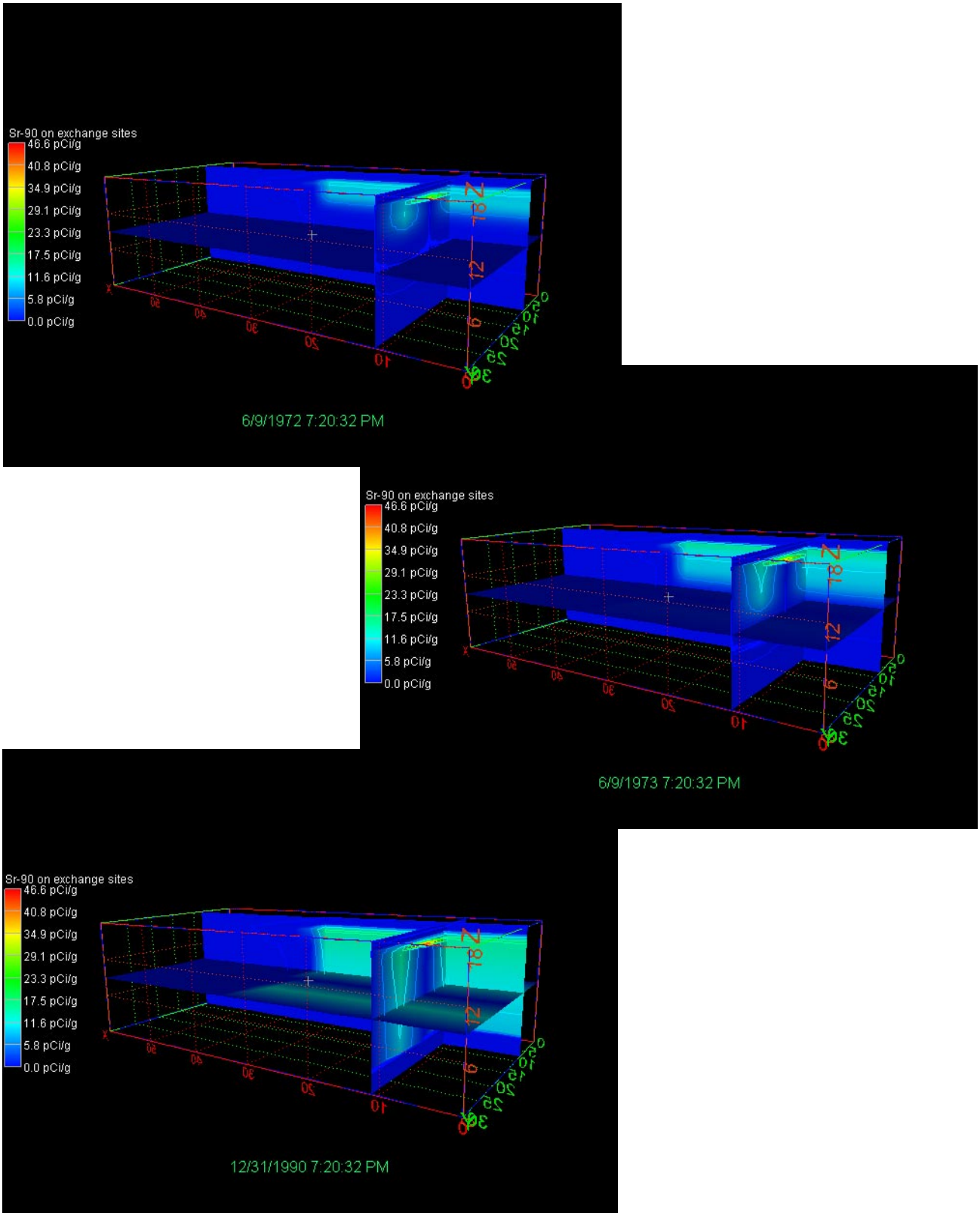

Figure J-10-14. Sr90 on the exchange sites 1,2, and 3 years after the CPP-31 release with CEC = 7 meq/100 g.

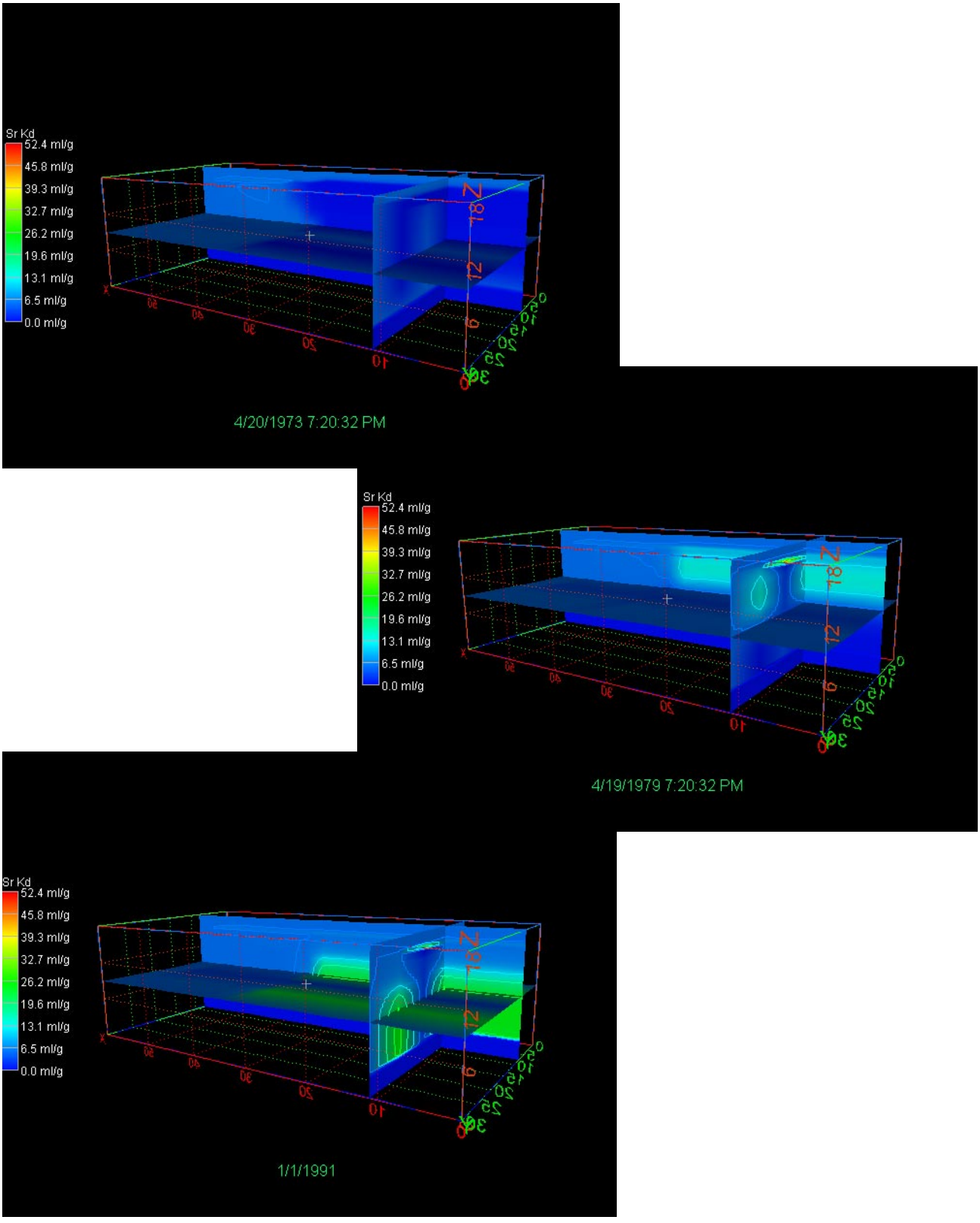

Figure J-10-15. Effective partitioning between aqueous and solid-phase Sr-90 0.5, 1.5, and 17.5 years after CPP-31 release with CEC = 7 meq/100 g.

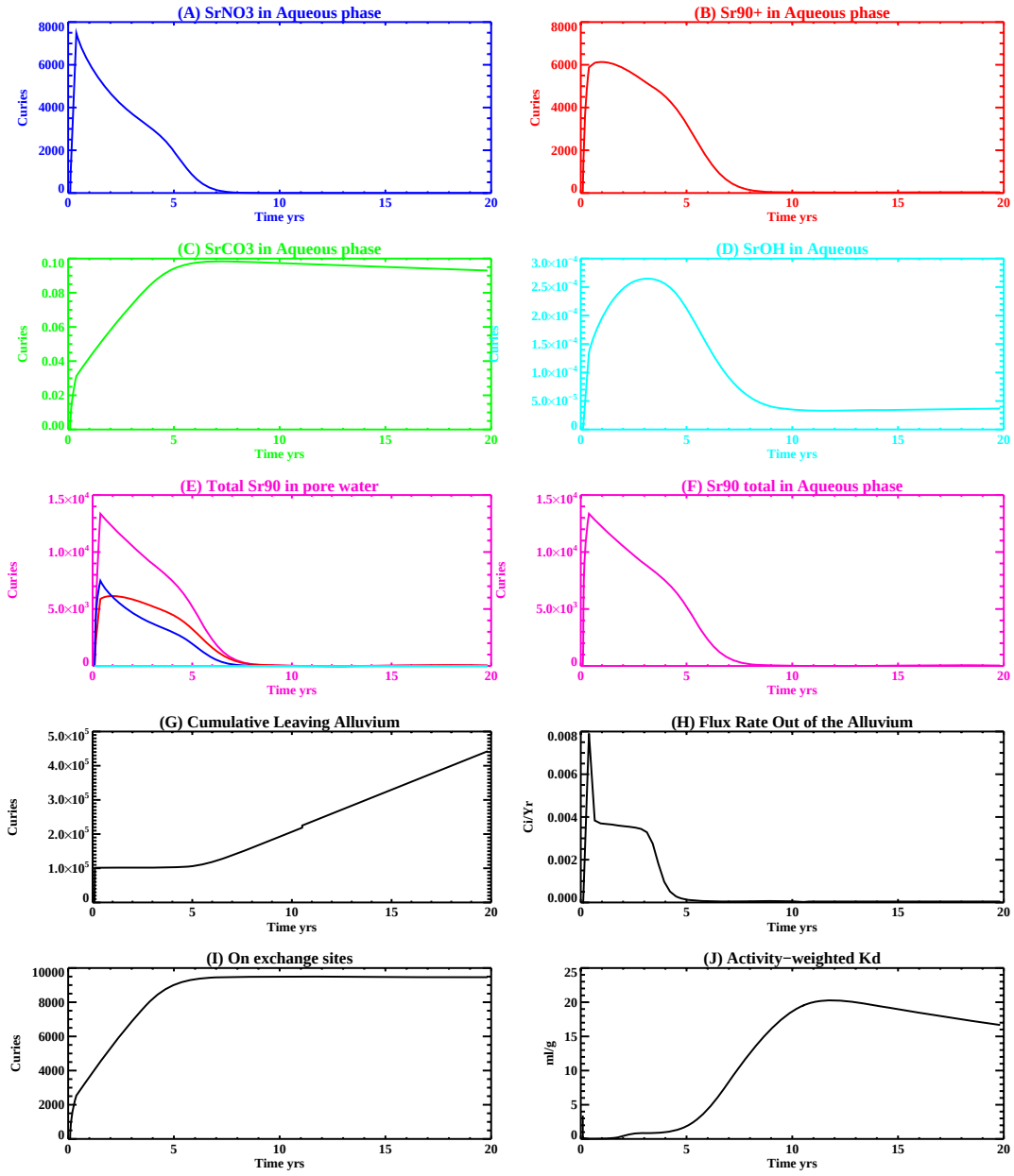

Figure J-10-16. Summary figure illustrating the speciation of Sr-90 in the aqueous phase (A-F), total Sr-90 in the pore-water of the alluvium (E), cumulative curies of Sr-90 having left the alluvium (G), flux rate leaving the alluvium (H), Sr-90 on the exchange sites (I), and effective partitioning coefficient (Kd) (J).

J-10.2.2 Vadose Zone Sr-90 Simulation Results

The release of Sr-90 in this simulation followed the same procedure as was used in the sensitivity base-case:

- 15900 Ci from CPP-31 release in the tank farm were represented using (a) the activity-release function shown in Figure J-10-16 (H) for the 6403 Ci released during the first 20 years, and placing this activity flux directly above the basalt interface of the base model (Appendix A, Section 5.1). The remaining 9497 Ci were distributed vertically through the alluvium scaled to the measured soil concentrations obtained during the 2004 sampling cycle (Appendix G and Table 5-32). To simulate the transport of the activity remaining in the alluvium, an effective K_d of 17 mL/g was used (Figure J-10-16 (J)) for the alluvium sediments.
- transport of Sr-90 from sources other than CPP-31 originating in the alluvium, whose location is spanned by the submodel (Appendix A, Section 5.1), were simulated using the submodel. Because these source locations were outside the influence of the high ionic strength, acidic CPP-31 release, a K_d of 20 mL/g was used in the submodel alluvium.
- transport of Sr-90 from sources located outside of the submodel horizontal extent were also placed in the base model used to simulate the transport of the CPP-31 remaining in the alluvium. The effective K_d for the alluvium underlying these source locations was also set to the value used to simulate the transport of Sr-90 predicted to remain in the alluvium after 20 yrs (first bullet). The relative magnitude of these sources are small relative to the residual Sr-90 predicted to remain in the alluvium after 20 yrs. In this case, the K_d is about equal to the value used to simulate the transport of Sr-90 from sources within the submodel boundary.

Figures J-10-17 through J-10-20 illustrate the distribution of the Sr-90 in the vadose zone through the year 2293 and the arrival of Sr-90 for key perched water wells is shown in Figure J-10-21. The subplots presented in Figure J-10-21 suggest that the model is predicting concentrations in the northern upper shallow wells quite well, however, concentrations in the northern lower shallow and northern deep perched water are not matched as well as they were in the RI/BRA base case. Specifically, comparisons to field data for wells near the former percolation ponds are much worse because of the increase in alluviul K_d (see Figure J-10-22). By comparing the predicted concentrations for wells near the percolation ponds obtained in simulations using 2, 3, and 7 meq/100g simulations, the better match to field data was obtained with the lower CEC values. Based on this observation, a reasonable K_d for the alluvium near the percolation ponds would be 2 mL/g which is consistent with the analyses of alluvial K_d presented in Section J-4.3, and suggests that the percolation pond water influences transport in that area.

Peak vadose zone concentrations through time are shown in red in Figure J-10-23 and are lower than the values predicted using the RI/BRA model (black) throughout most of the simulation time period. The largest deviations occur near the time of the highest vadose zone concentrations when they are 25% of those obtained in the RI/BRA model. It is apparent from this that the highest concentrations actually occur in the pore water of the alluvium.

The rate at which Sr-90 activity enters the aquifer is represented by the red line in Figure J-10-24, and can be compared directly to the RI/BRA model (black) results. Relative to the RI/BRA model, increasing the CEC has resulted in:

- 52% as much Sr-90 leaving the alluvium in the first 20 years (6403 vs. 12336)
- 267% as much Sr-90 remaining in the alluvium (9497 Ci vs. 3564 Ci)
- decreased mobility of Sr-90 due to an increase in K_d (17 mL/g vs. 2 mL/g)

The higher K_d used to simulate the transport of the Sr-90 remaining in the alluvium means that the peak aquifer concentrations can be attributed solely to the Sr-90 originating at non-CPP-31 sources added to those attributable to the 6403 Ci released during the first 5 years. This has important implications with respect to the fate of Sr-90 remaining in the alluvium, and suggests that although there is a larger source remaining in the

alluvium, that it does not appreciably increase the total activity leaving the vadose zone. This is apparent in Figure J-10-24 where the difference in the flux of activity into the aquifer between the base case and this simulation is primarily due to differences occurring during first 5 years.

Figure J-10-17. Sr-90 vadose zone concentration with an alluvial CEC=7 meq/100 g (horizontal contours) (pCi/L) (MCL = thick red line, 10*MCL = thin red line, MCL/10 = black line).

Figure J-10-18. Sr-90 vadose zone concentration with an alluvial CEC=7 meq/100 g (horizontal contours) (pCi/L) (MCL = thick red line, 10*MCL = thin red line, MCL/10 = black line).

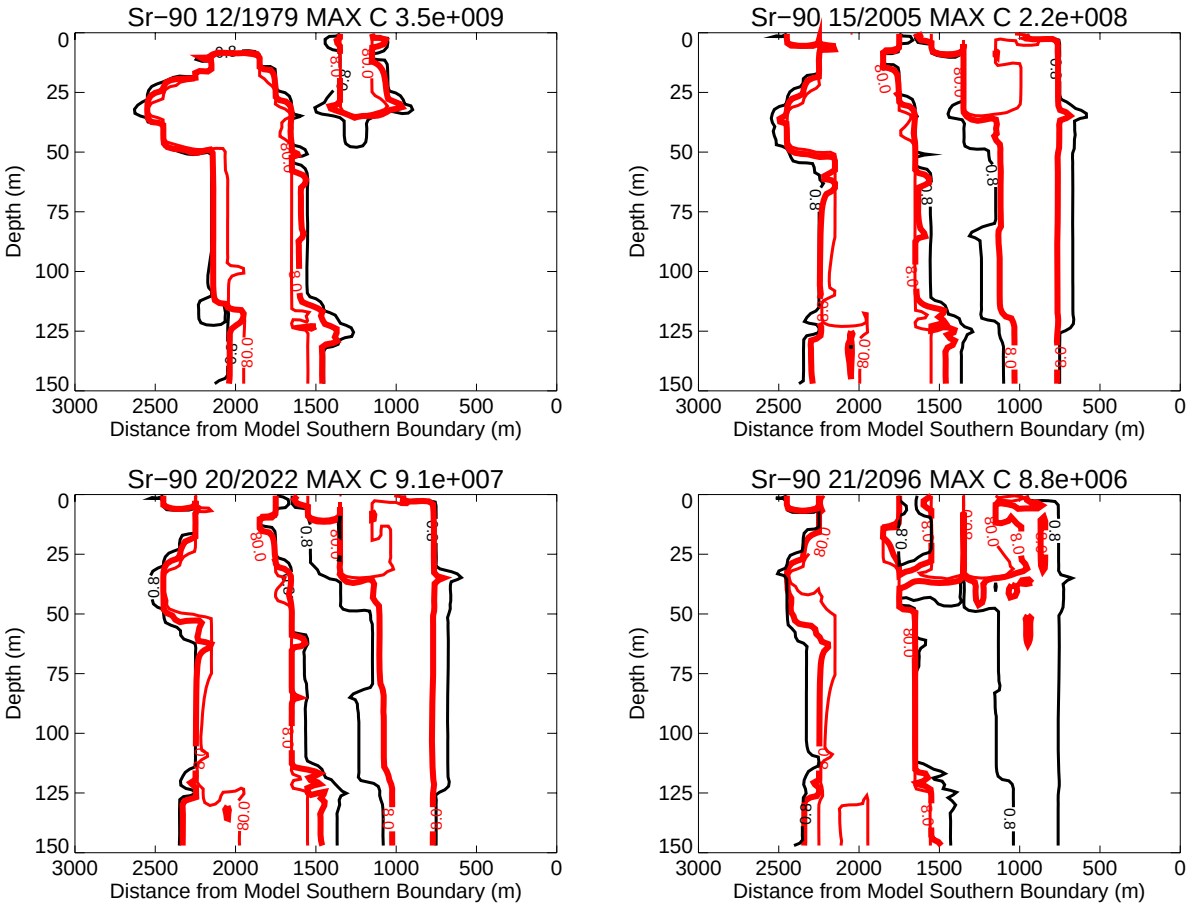

Figure J-10-19. Sr-90 vadose zone concentrations with an alluvial CEC=7 meq/100 g (vertical contours) (pCi/L) (MCL = thick red line, 10*MCL = thin red line, MCL/10 = black line).

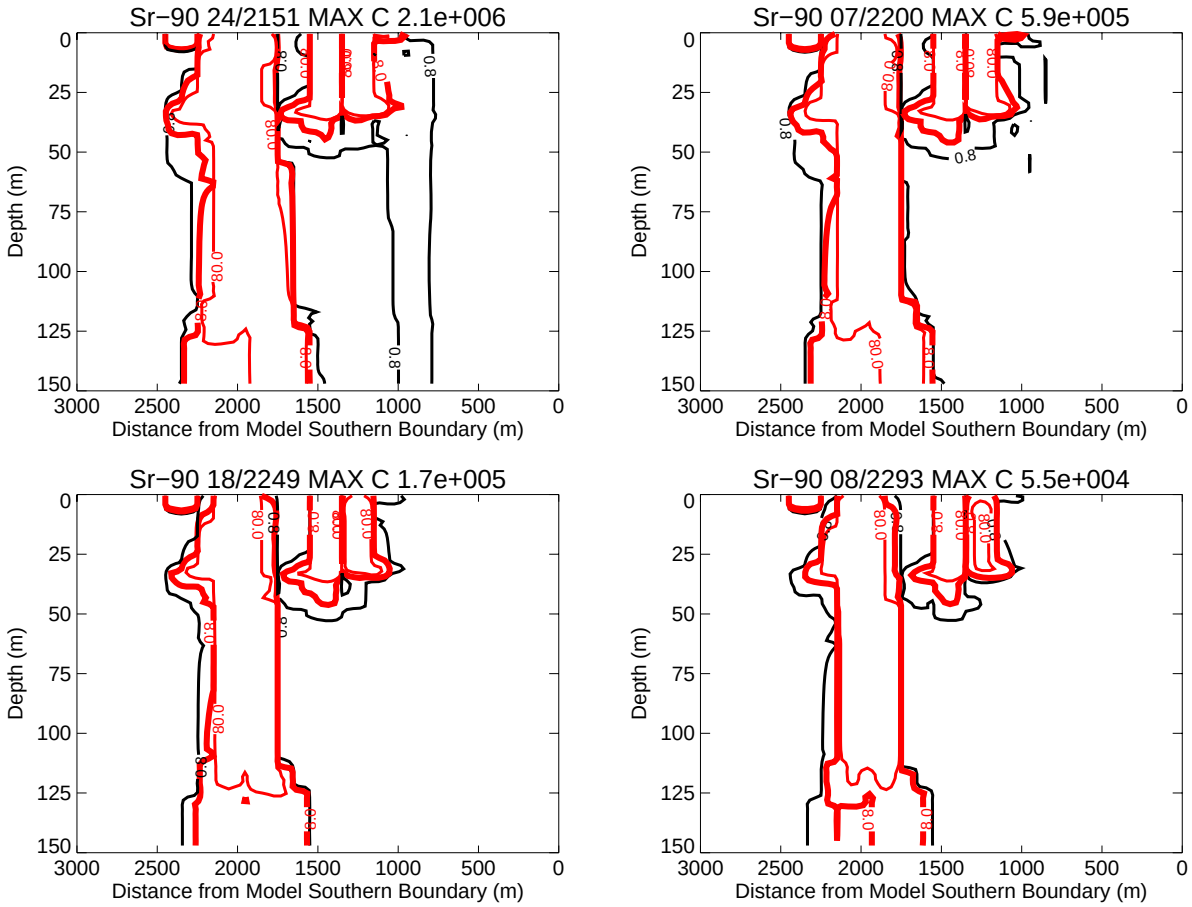

Figure J-10-20. Sr-90 vadose zone concentrations with an alluvial CEC=7 meq/100 g (vertical contours) (pCi/L) (continued) (MCL = thick red line, 10*MCL = thin red line, MCL/10 = black line).

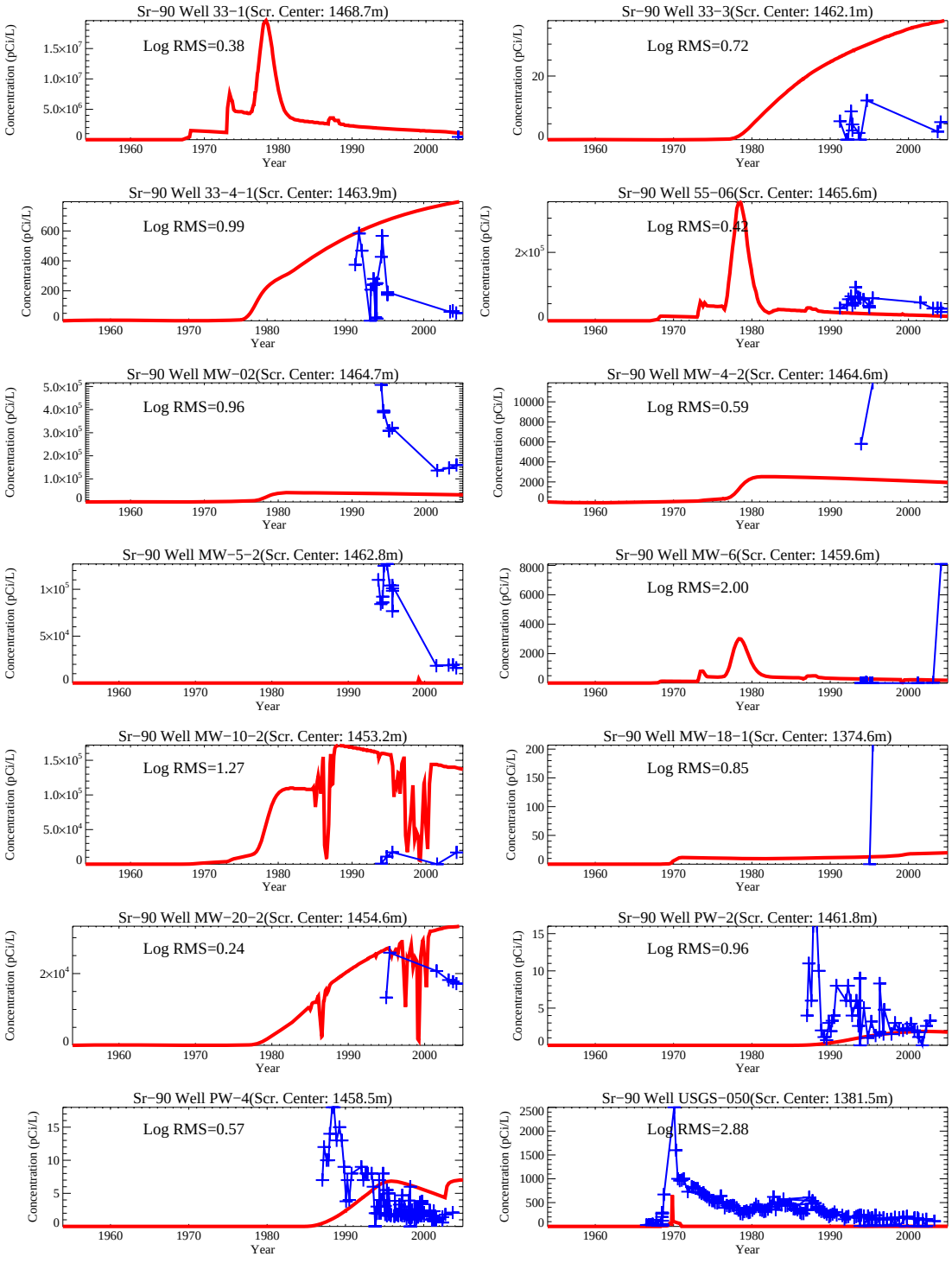

Figure J-10-21. Sr-90 concentration in perched water wells with an alluvial CEC=7 meq/100 g (pCi/L) (Measured values = blue crosses, red = model at screen center).

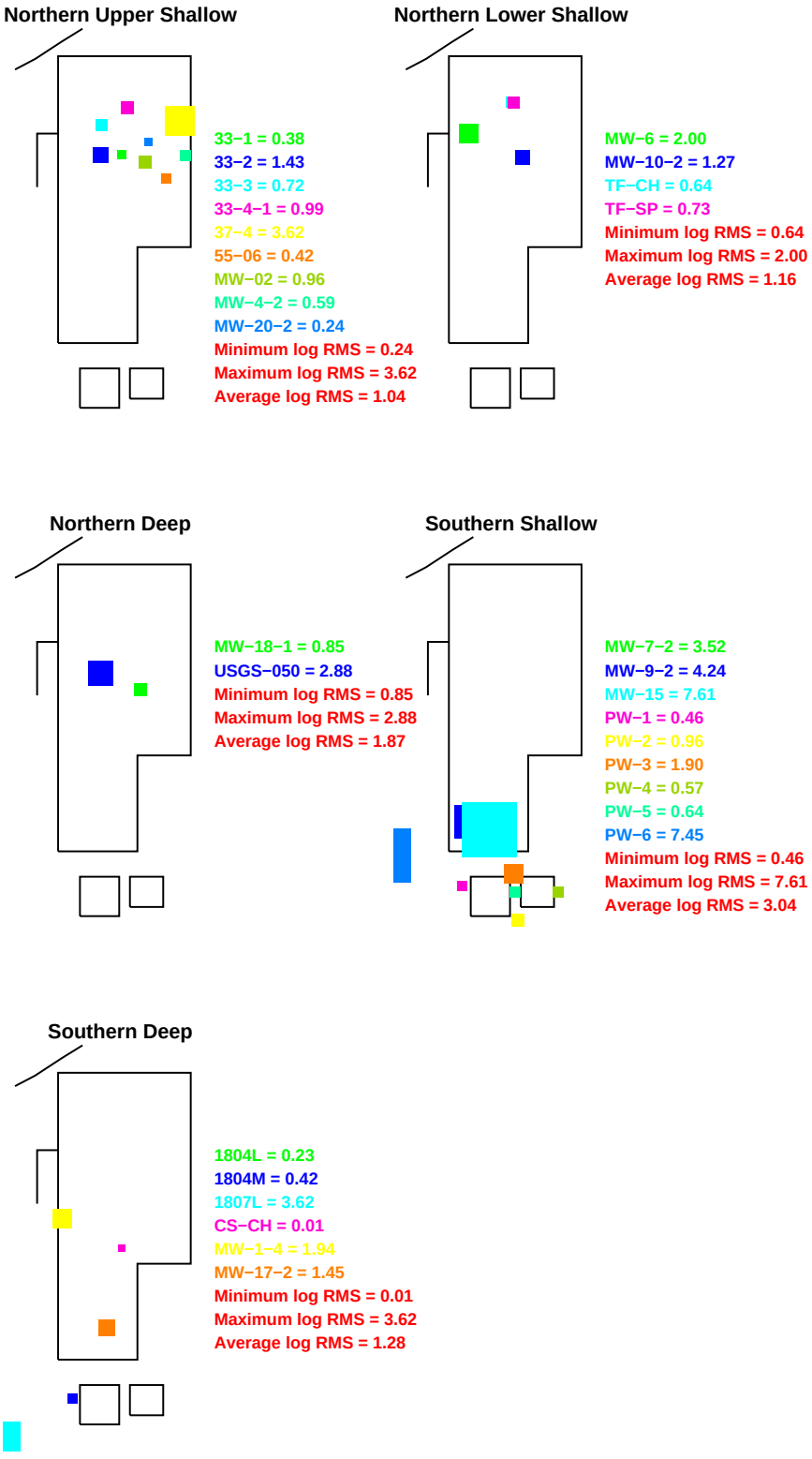

Figure J-10-22. Log 10 Root mean square error (RMS) by depth and northing with an alluvial CEC=7 meq/100 g.

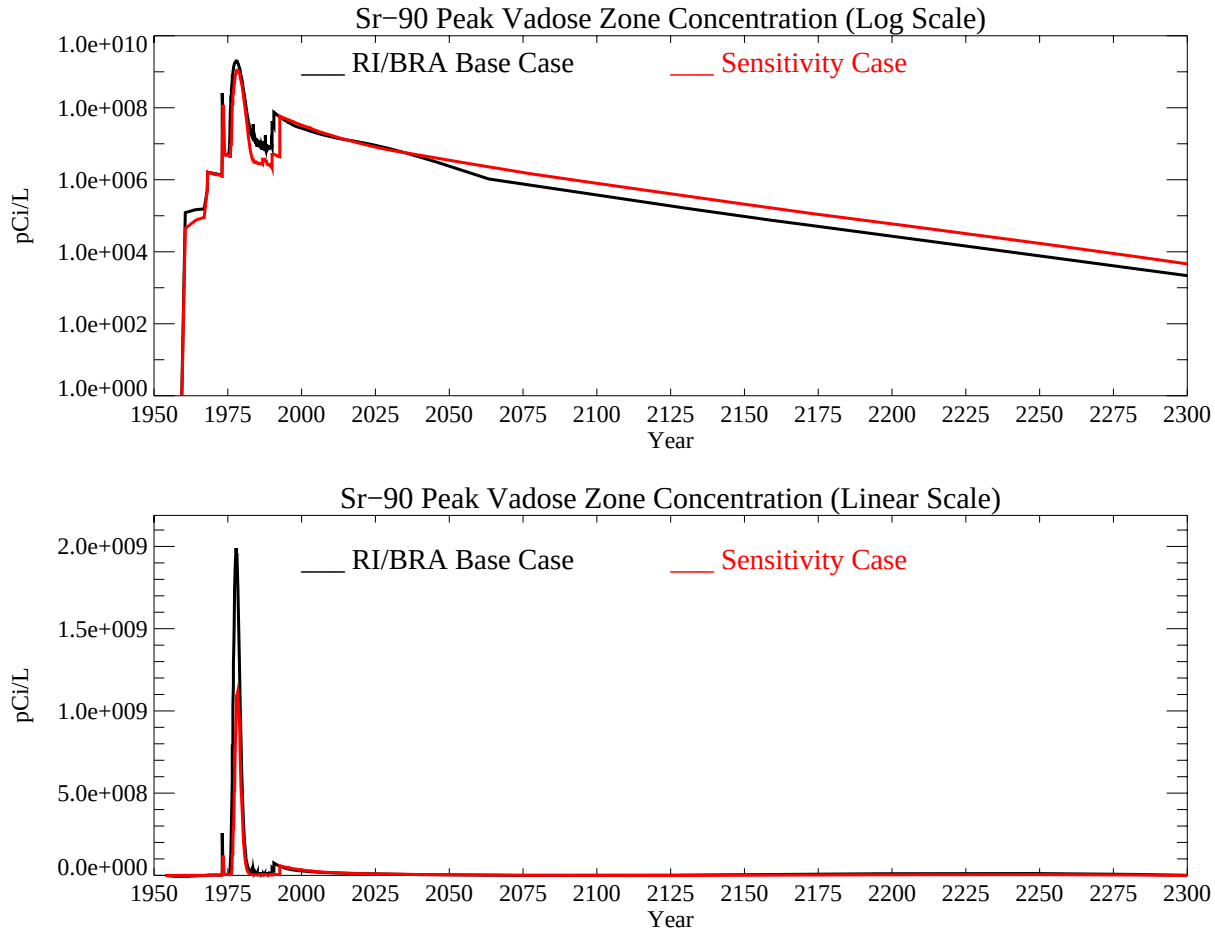

Figure J-10-23. Sr-90 peak vadose zone concentrations with an alluvial CEC=7 meq/100 g (pCi/L) with the RI/BRA model in black and this sensitivity run in red.

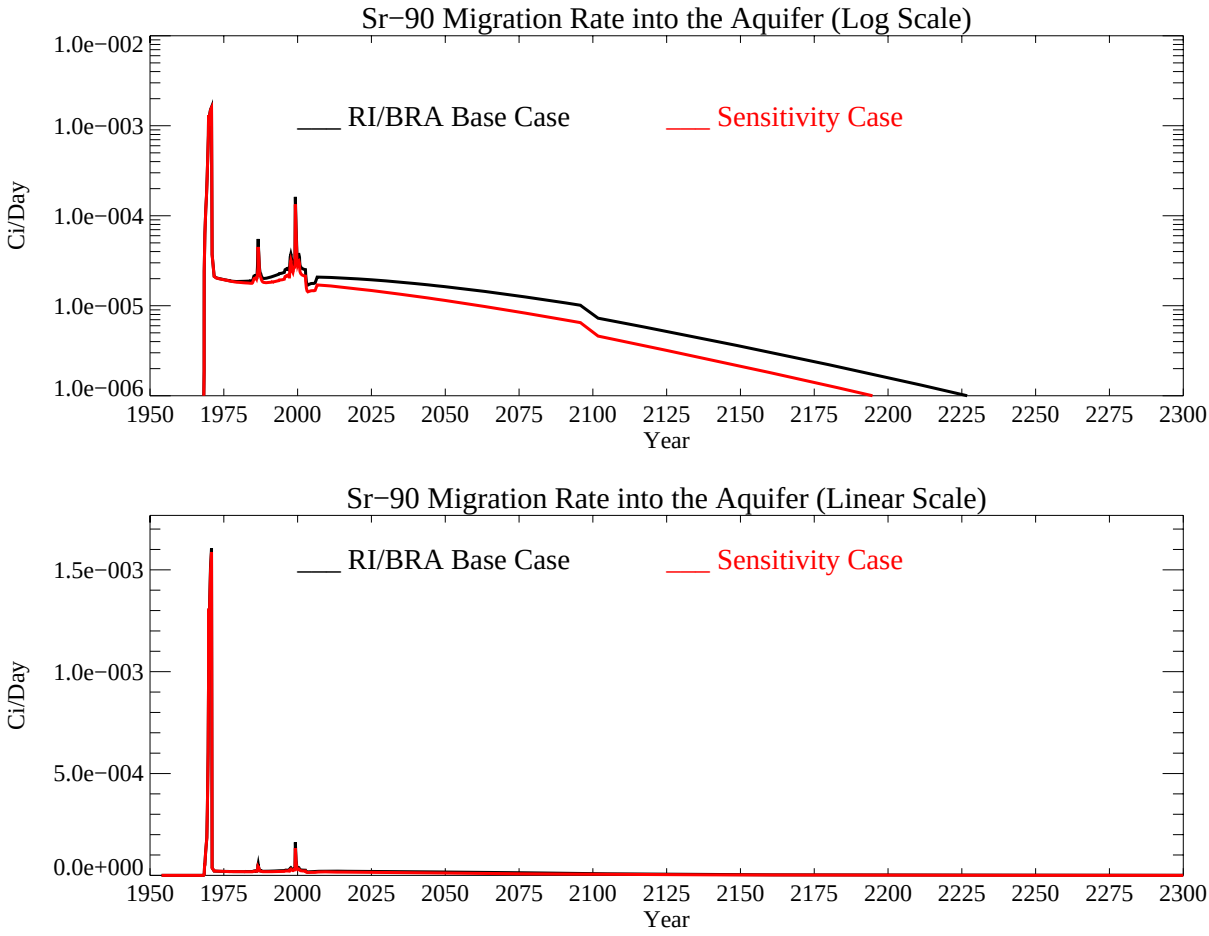

Figure J-10-24. Sr-90 activity flux into the aquifer with an alluvial CEC=7 meq/100 g (Ci/day) with the RI/BRA model in black, and this sensitivity run in red.

J-10.2.3 Aquifer Sr-90 Simulation Results

The distribution Sr-90 in the aquifer for the time period spanning 2005-2096 is given on the course grid in Figure J-10-25 and on the fine grid in Figure J-10-26 for times spanning 2049-2151. The resultant peak aquifer concentrations are given in Figure J-10-27. Because the Sr-90 originating in the vadose zone does not arrive in the aquifer until the mid 1980's, comparisons to measured data are not presented for aquifer wells.

The three important performance measures are concentrations beyond 2095, the spatial extent of contamination, and the time period during which concentrations exceed the MCL. The predicted peak Sr-90 concentration in the year 2095 is 11.5 pCi/L, 60% of that predicted in the RI/BRA model. This concentration exceeds the MCL by a factor of 1.5, with the majority of the long-term impact originating from the initial rapid release of Sr-90 from the tank farm. If there were a significant contribution from the larger activity remaining at the surface, the deviation between RI/BRA and this model peak concentrations would increase over time. The absence of increased deviation confirms that the Sr-90 remaining adsorbed to the alluvial sediments is not significantly contributing to aquifer concentrations later in time.

The Sr-90 contour plots presented in Figures J-10-25 and J-10-26 suggest that the predicted distribution in the aquifer after 2000 does not differ greatly from that predicted in the RI/BRA model. Although Sr-90 concentrations in the aquifer are predicted to exceed the MCL beyond 2095, the area impacted by Sr-90 above 8 pCi/L is well within the INTEC fence line by 2049.

The time during which the MCL is exceeded in this case (year 2105) is significantly sooner than obtained in the RI/BRA model (2129).

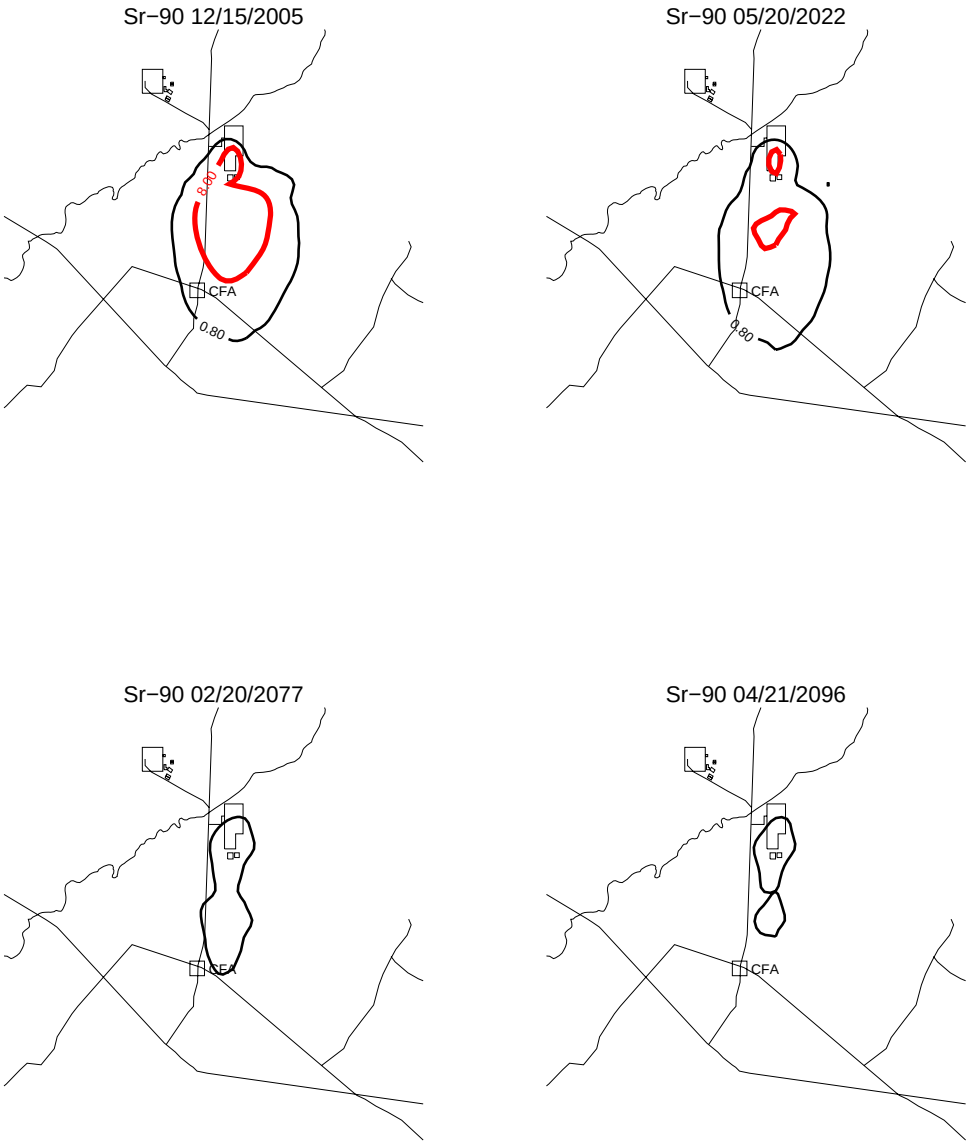

Figure J-10-25. Sr-90 aquifer concentration contours with an alluvial CEC=7 meq/100 g (pCi/L) (MCL = thick red line, 10*MCL = thin red line, MCL/10 = black line).

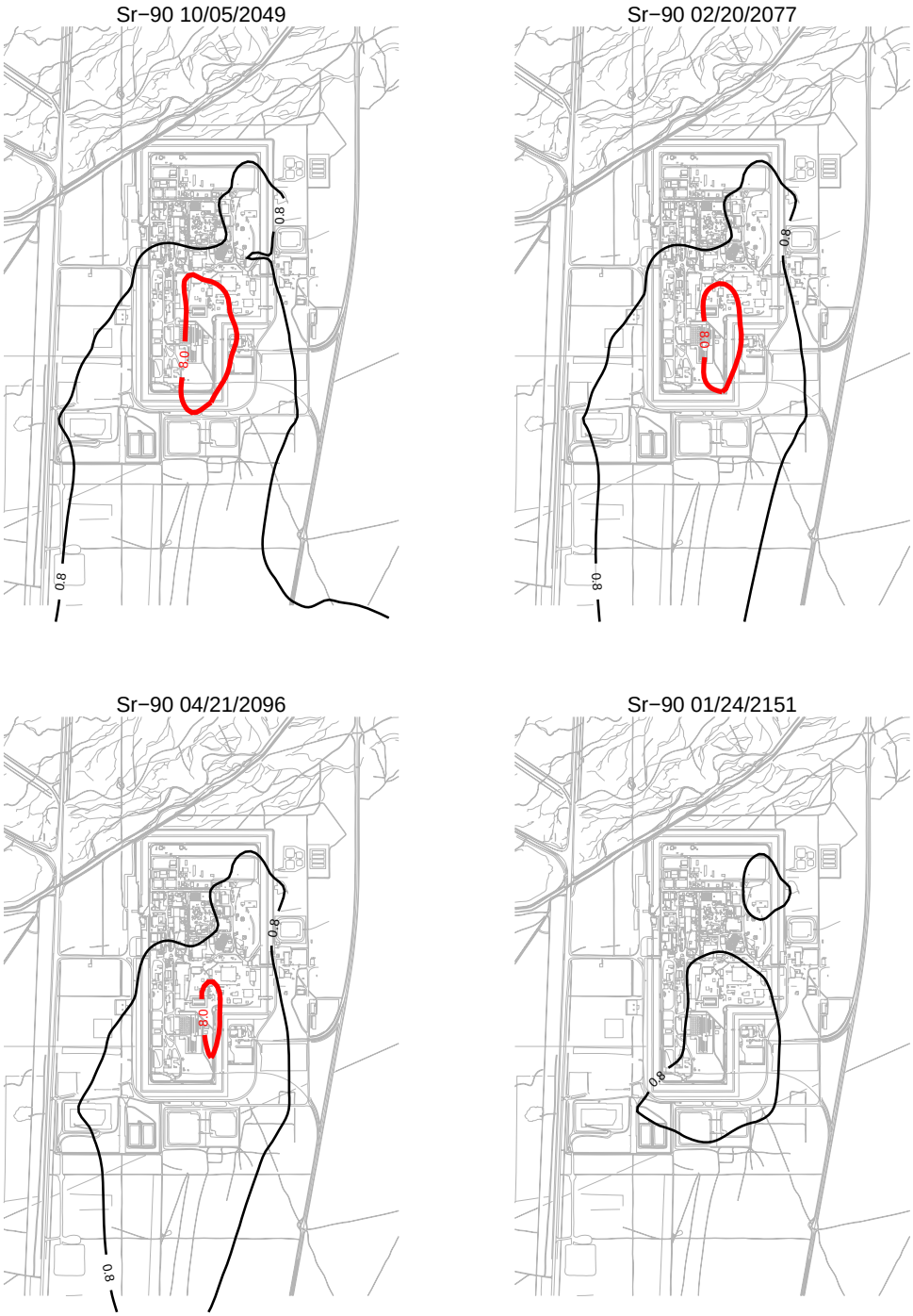

Figure J-10-26. Sr-90 aquifer concentration contours with an alluvial CEC=7 meq/100 g (pCi/L) (continued) (MCL = thick red line, 10*MCL = thin red line, MCL/10 = black line).

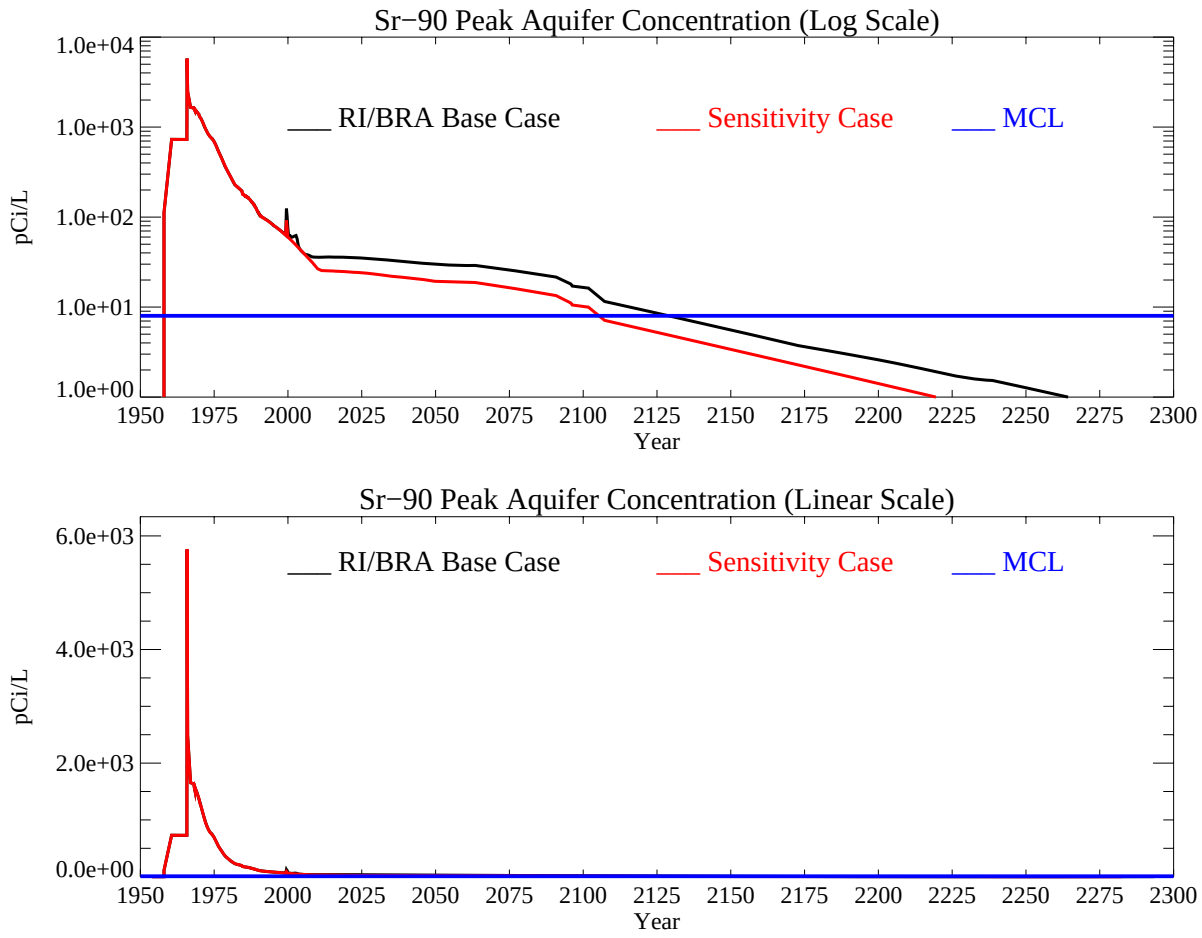

Figure J-10-27. Sr-90 peak aquifer concentrations with an alluvial CEC=7 meq/100 g (pCi/L) with the MCL in blue, RI/BRA model in black and this sensitivity run in red.

J-10.3 Decreased Interbed K_d of 22 mL/g

The previous two simulations examined the resulting uncertainty in predicted vadose zone and aquifer concentrations that are associated over the range of CECs in the alluvium. The interbed materials are also variable, with a smaller expected range in adsorptive capacity. Less variability occurs primarily as a result of a narrower size fractionation, with the material being much finer. As discussed in Section J-6, the K_d used in the RI/BRA model is representative of the mid-range K_d of 50 mL/g. This sensitivity study examines the impact of using a K_d on the low end of the expected range, with this value equal to 22 mL/g.

J-10.3.1 Geochemical Evolution in the Alluvium

This sensitivity simulation uses the geochemical results obtained for the RI/BRA base case simulation presented in Section J-8. In the RI/BRA model, 12336 Ci were released in the first 20 years, with 3564 Ci remaining in the alluvium with a K_d of 2 mL/g. The difference between this simulation and the sensitivity base case is solely due to the decreased interbed K_d.

J-10.3.2 Vadose Zone Sr-90 Simulation Results

The release of Sr-90 in this simulation followed the same procedure as was used in the RI/BRA model:

- 15900 Ci from CPP-31 release in the tank farm were represented using (a) the activity-release function shown in Figure J-8-9 (H) for the 12336 Ci released during the first 20 years, and placing this activity flux directly above the basalt interface of the base model (Appendix A, Section 5.1). The remaining 3564 Ci were placed roughly mid way through the alluvium, corresponding to the location of the peak measured soil concentrations obtained during the 2004 (Appendix G and Table 5-32) sampling cycle. To simulate the transport of the activity remaining in the alluvium, an effective K_d of 2 mL/g was used (Figure J-8-9 (J)) for the alluvium sediments.
- transport of Sr-90 from sources other than CPP-31 originating in the alluvium, whose location is spanned by the submodel (Appendix A, Section 5.1), were simulated using the submodel. Because these source locations were outside the influence of the high ionic strength, acidic CPP-31 release, a K_d of 20 mL/g was used in the submodel alluvium.
- transport of Sr-90 from sources located outside of the submodel horizontal extent were also placed in the base model used to simulate the transport of the CPP-31 remaining in the alluvium. The effective K_d for the alluvium underlying these source locations was also set to the value used to simulate the transport of Sr-90 predicted to remain in the alluvium after 20 yrs (first bullet). The relative magnitude of these sources are small relative to the residual Sr-90 predicted to remain in the alluvium after 20 yrs.

The distribution of Sr-90 in the vadose zone is shown through year 2293 in Figures J-10-28 through J-10-31. The arrival of Sr-90 in key perched water wells is compared to field data in Figure J-10-32, and is summarized for all wells in Figure J-10-33. The subplots presented in Figure J-10-32 suggest that the model is overpredicting concentrations in most of the higher concentration upper shallow perched water wells. The wells near the former percolation ponds also have a poorer match because of the decreased interbed K_d. The worst matches occur in the deeper wells because Sr-90 can migrate from the shallow higher concentration regions, resulting in general overprediction at depth.

Peak vadose zone concentrations through time are shown in red in Figure J-10-34 and are about equal to those predicted in the RI/BRA base case through year 2050. This is an indication that these high vadose zone concentrations are in the alluvium because the lower interbed K_d would allow perched water concentrations to increase above those predicted by the RI/BRA model.

The rate at which Sr-90 enters the aquifer (red) is given in Figure J-10-35, and can be compared directly to the RI/BRA model predictions (black). Clearly, decreasing the interbed K_d has had a significant impact on the expected migration of Sr-90 into the aquifer, with this impact occuring throughout the entire simulation period. The distribution coefficient is essentially the ratio of mass (activity) adsorbed on the exchange sites to that in the aqueous phase. As the K_d decreases, the aqueous phase concentration increases. Applying the smaller K_d to all of the interbed sediments allows less adsorption of total Sr-90 activity throughout the vadose zone, including the deeper interbeds affected by the failed CPP-03 injection well. The lower K_d increases the downward migration of Sr-90 and allows less decay to occur en route to the aquifer. The flux rate predicted using a K_d of 22 mL/g is much higher than predicted in the RI/BRA model.

Figure J-10-28. Sr-90 vadose zone concentration assuming an interbed K_d=22 mL/g (horizontal contours) (pCi/L) (MCL = thick red line, 10*MCL = thin red line, MCL/10 = black line).

Figure J-10-29. Sr-90 vadose zone concentration assuming an interbed K_d=22 mL/g (horizontal contours) (pCi/L) (MCL = thick red line, 10*MCL = thin red line, MCL/10 = black line).

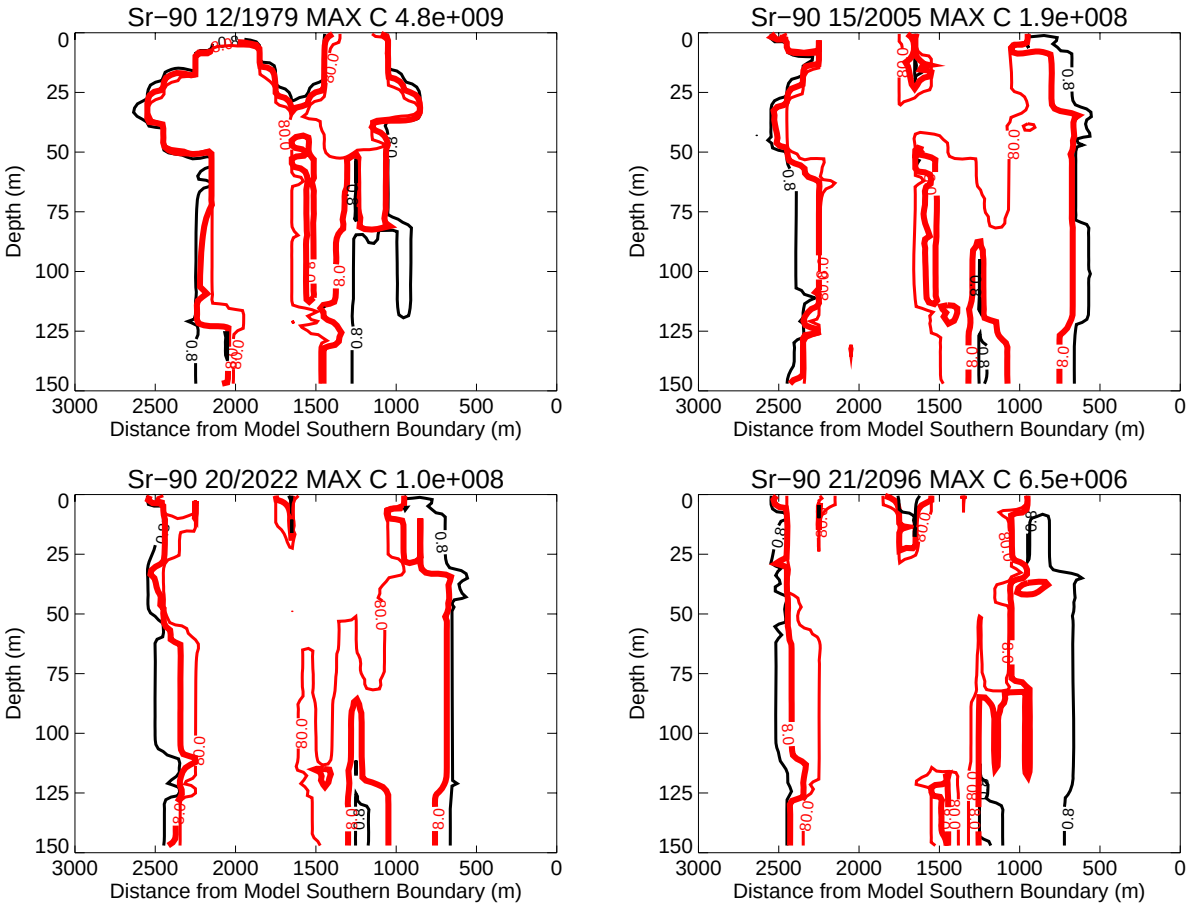

Figure J-10-30. Sr-90 vadose zone concentrations assuming an interbed K_d=22 mL/g (vertical contours) (pCi/L) (MCL = thick red line, 10*MCL = thin red line, MCL/10 = black line).

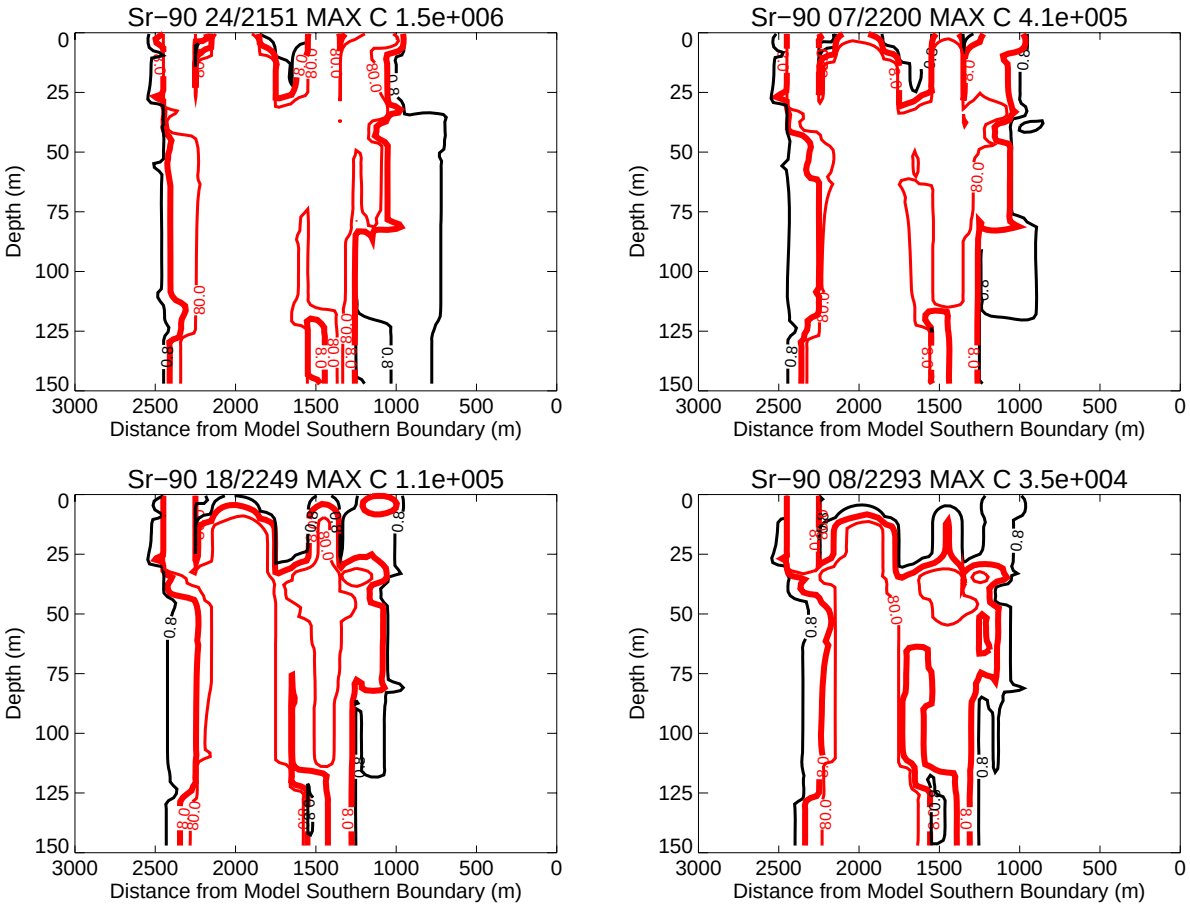

Figure J-10-31. Sr-90 vadose zone concentrations assuming an interbed K_d=22 mL/g (vertical contours) (pCi/L) (continued) (MCL = thick red line, 10*MCL = thin red line,

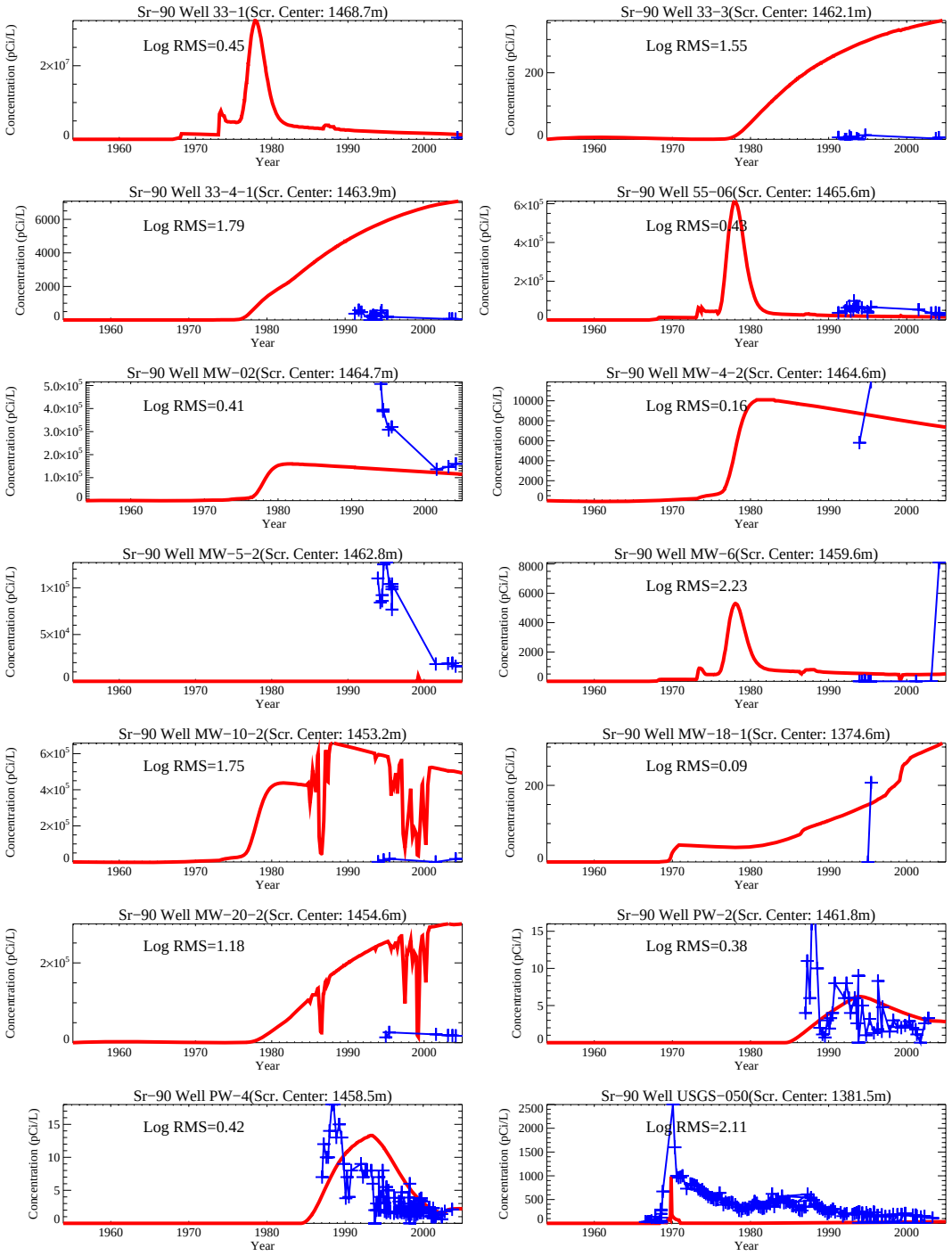

Figure J-10-32. Sr-90 concentration in perched water wells assuming an interbed K_d=22 mL/g (pCi/L) (Measured values = blue crosses, red = model at screen center).

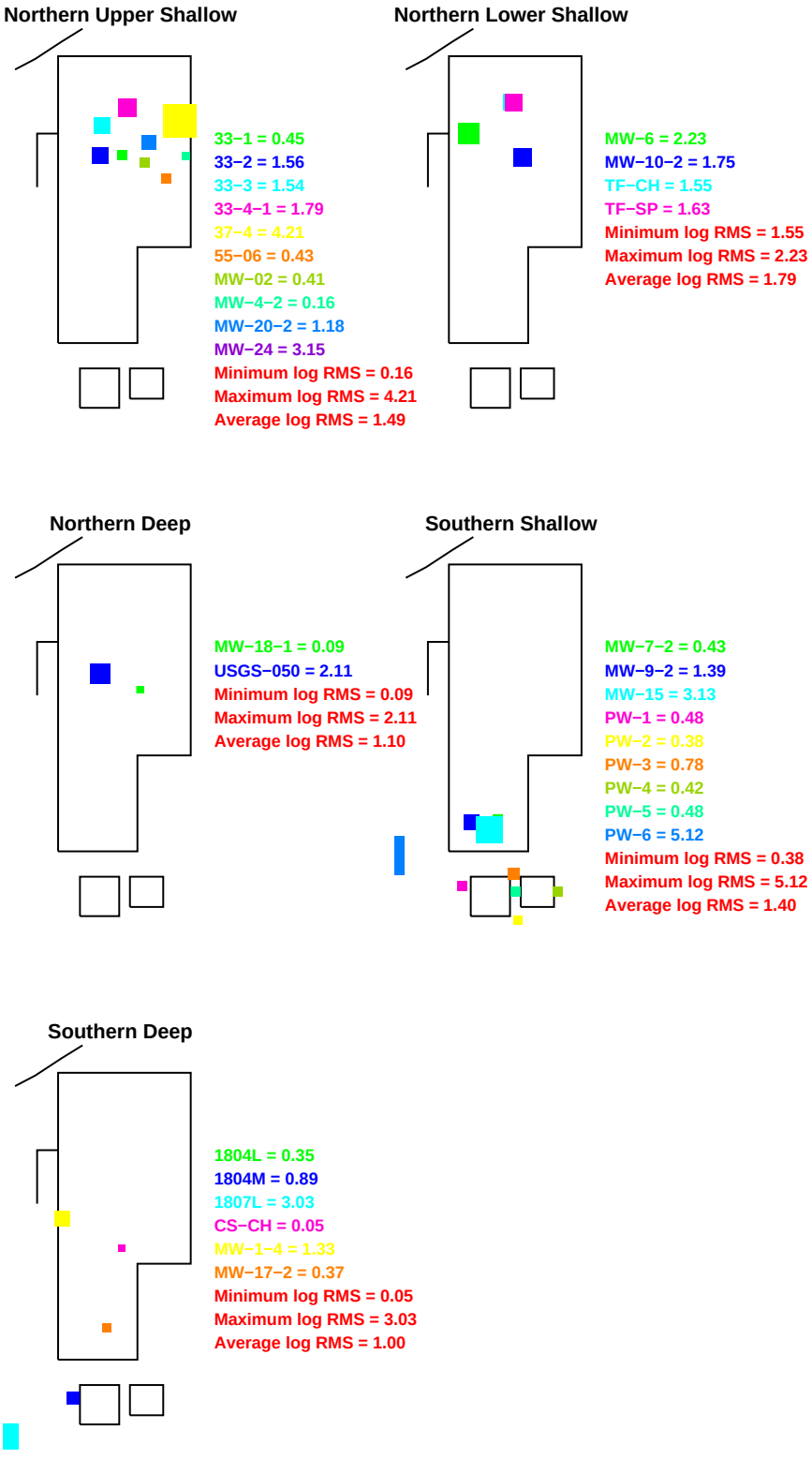

Figure J-10-33. Log 10 Root mean square error (RMS) by depth and northing assuming an interbed K_d=22 mL/g.

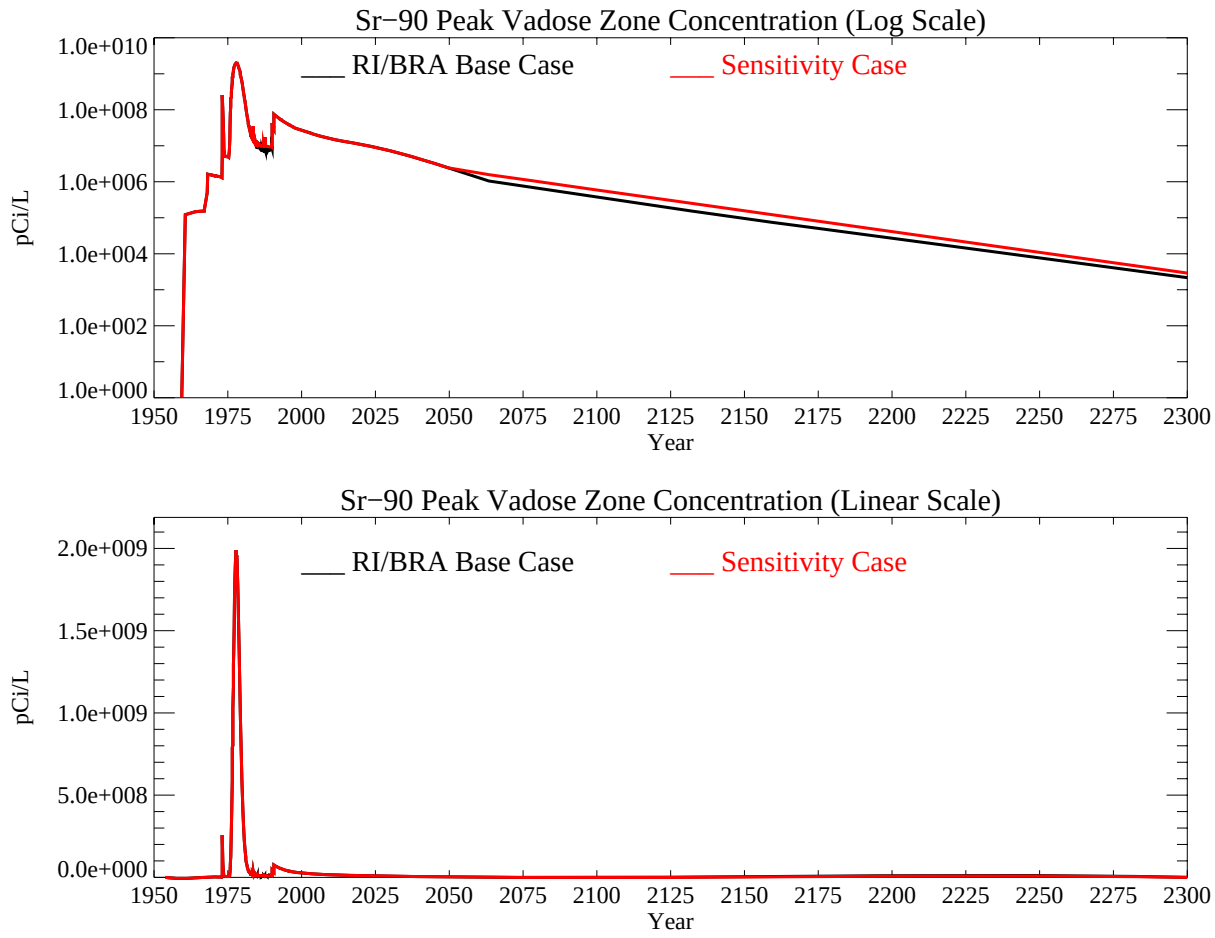

Figure J-10-34. Sr-90 peak vadose zone concentrations assuming an interbed K_d=22 mL/g (pCi/L) with the RI/BRA model in black and this sensitivity run in red.

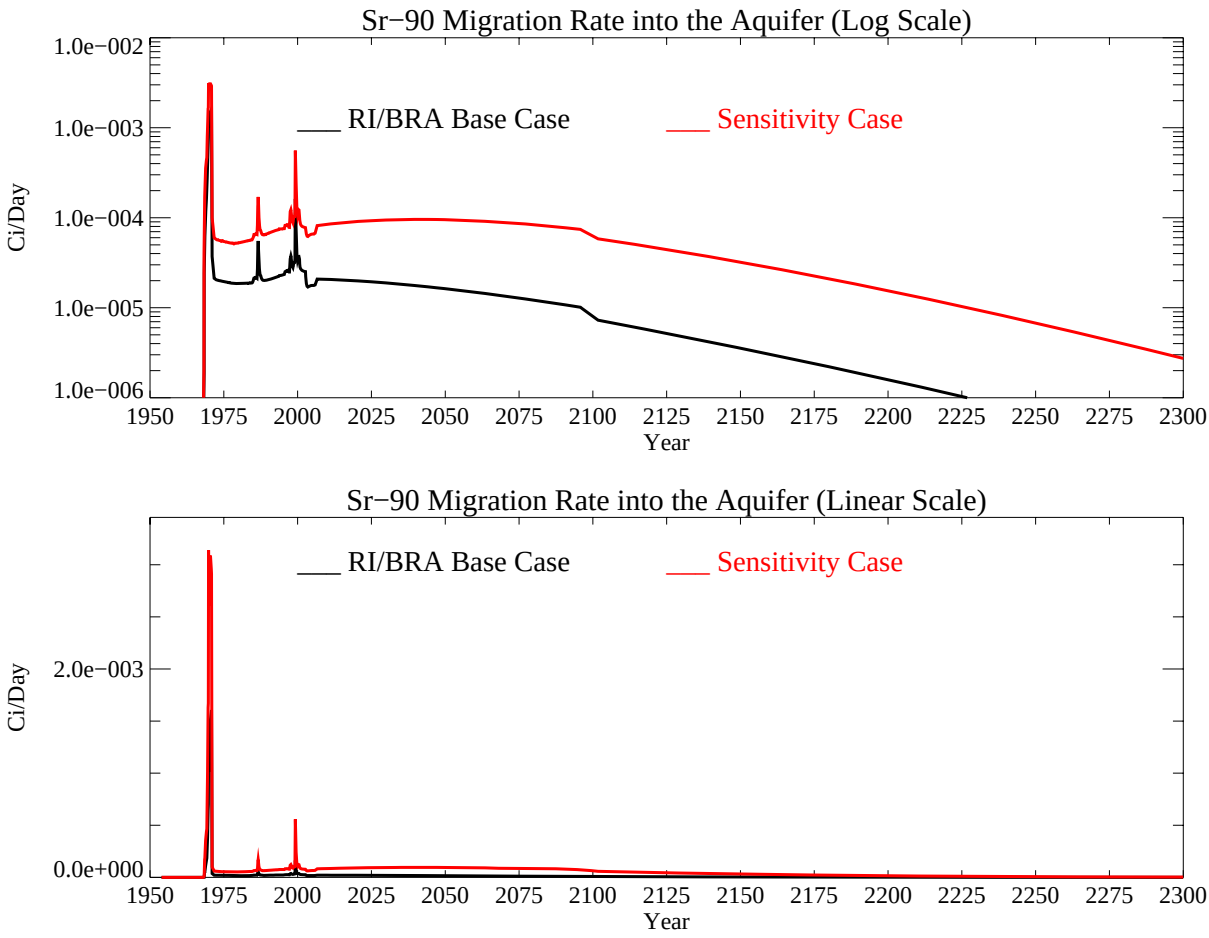

Figure J-10-35. Sr-90 activity flux into the aquifer assuming an interbed K_d=22 mL/g (Ci/day) with the RI/BRA base case in black, and this sensitivity run in red.

J-10.3.3 Aquifer Sr-90 Simulation Results

On the course grid, the distribution Sr-90 in the aquifer for the time period spanning 2005-2096 is given in Figure J-10-36. Figure J-10-37 contains the contours on the fine grid for the 2049-2151 time period. Resultant peak aquifer concentrations are given in Figure J-10-38. Because the Sr-90 originating in the vadose zone does not arrive in the aquifer until the mid 1980's, comparisons to measured data are not presented for aquifer wells.

The three performance measures are peak concentration in 2095, area impacted above the MCL, and time during which the MCL is exceeded. Decreasing the interbed Kd by a factor of 2.3 has increased the peak concentration in 2095 to 110.8 pCi/L, about six times that predicted for the sensitivity base case (18.6 pCi/L). The nonlinearity is caused by the combination of increased flux rate out of the alluvium and lack of decay enroute. This difference is significant given overall model uncertainty.

There are also significant differences in the spatial distribution of Sr-90. The Sr-90 contour plots presented in Figures J-10-36 and J-10-37 show that Sr-90 concentrations in the aquifer are predicted to be extensive through out the presented time interval. The concentration isopleth representing the MCL is not contained within the intec facility boundaries until about 2151. This means that the flux rate of Sr-90 coming from the vadose zone is much higher than the dilution, retardation, and decay rates in the aquifer.

The simulated Sr-90 concentrations with this lower adsorption in the interbeds remain above the MCL from 1960 through year 2263. In the RI/BRA base-case, peak concentrations were not reduced below the MCL until year 2129. Decreasing the K_d by a factor of 2.3 keeps predicted Sr-90 concentrations in the aquifer above the MCL for an additional 134 years.

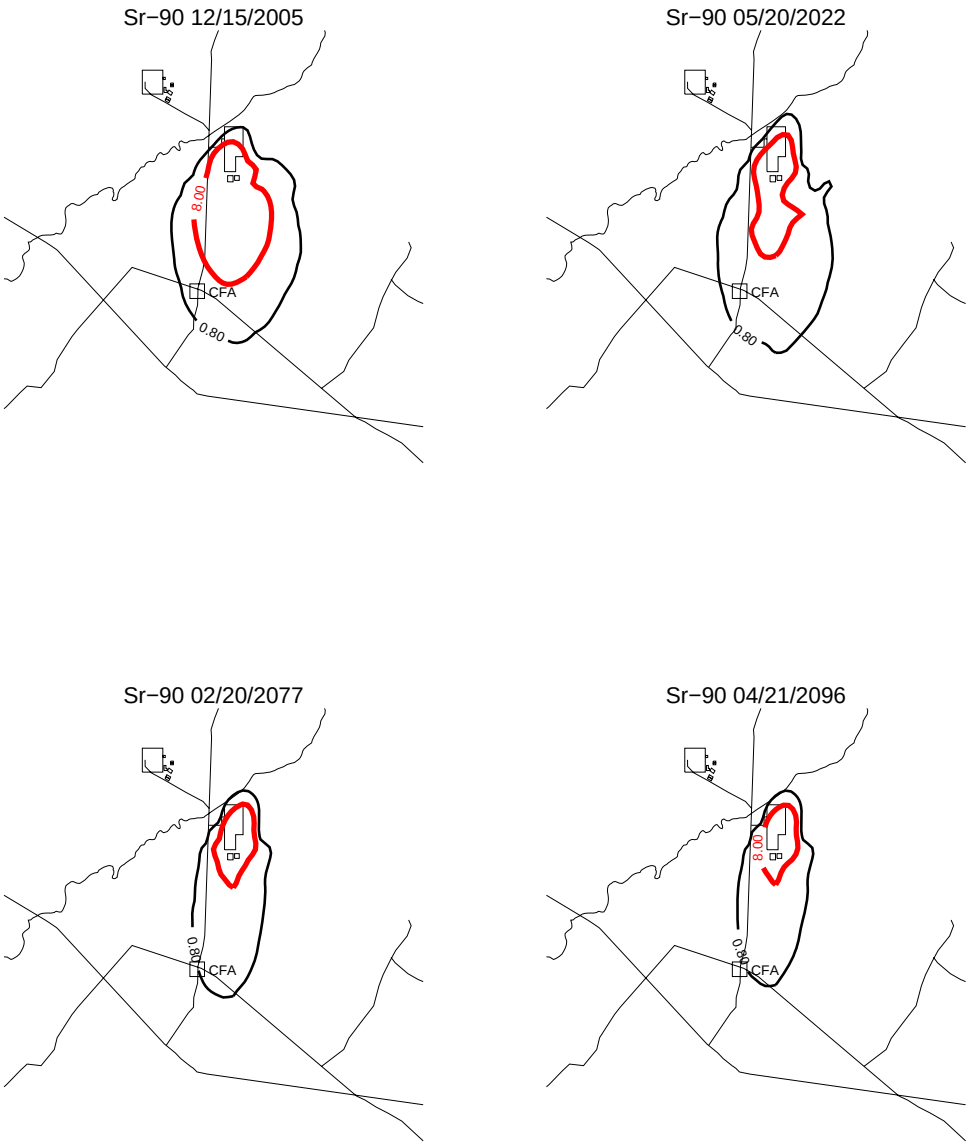

Figure J-10-36. Sr-90 aquifer concentration contours assuming an interbed K_d=22 mL/g (pCi/L) (MCL = thick red line, 10*MCL = thin red line, MCL/10 = black line).

Figure J-10-37. Sr-90 aquifer concentration contours assuming an interbed K_d=22 mL/g (pCi/L) (continued) (MCL = thick red line, 10*MCL = thin red line, MCL/10 = black line).

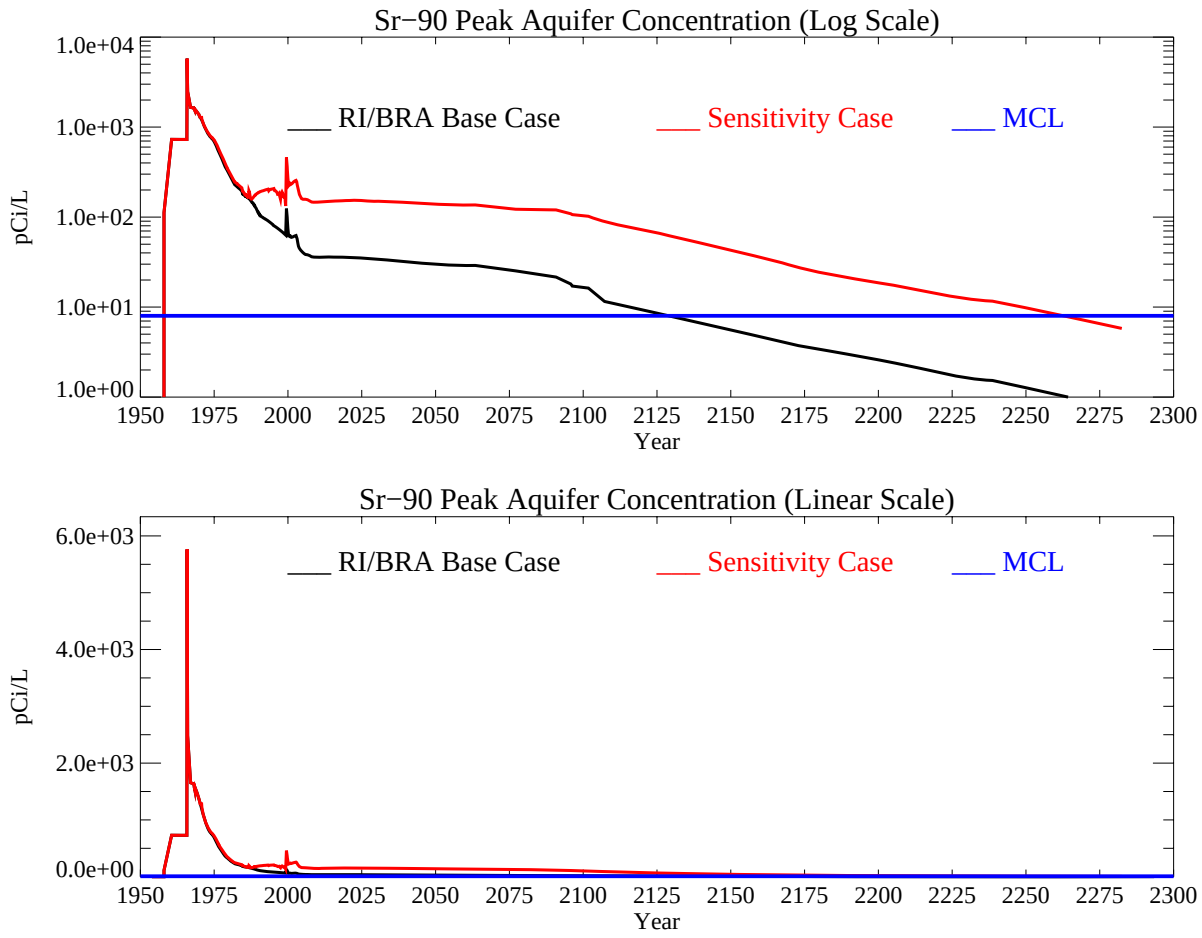

Figure J-10-38. Sr-90 peak aquifer concentrations assuming an interbed K_d=22 mL/g (pCi/L) with the MCL in blue, RI/BRA model in black and this sensitivity run in red.